PASJ: Publ. Astron. Soc. Japan **58**, 203–209, 2006 February 25

Polarization of Light from Warm Clouds above an Accretion Disk: Effects of Strong Gravity near a Black Hole

Jiří HORÁK and Vladimír KARAS
Astronomical Institute, Academy of Sciences, Boční II, CZ-141 31 Prague, Czech Republic

(Received 2005 November 17; accepted 2005 December 5)

Abstract

We consider polarization from the scattering of light on a cloud in radial motion along the symmetry axis of an accretion disk. Radiation drag from the disk and gravitational attraction of the central black hole are taken into account, as well as the effect of the cloud cooling in the radiation field. This provides us with a self-consistent toy-model for predicted lightcurves, including the linear polarization that arises from the scattering. Strong gravitational lensing creates indirect images; these are formed by photons that originate from the disk, become backscattered onto the photon circular orbit and eventually redirected toward an observer. Under suitable geometrical conditions the indirect photons may visibly influence the resulting magnitude of the polarization and light-curve profiles. Relevant targets are black holes in active galactic nuclei and stellar-mass Galactic black-holes exhibiting episodic accretion/ejection events.

Key words: accretion disks — black holes — general relativity — gravitational lensing — polarization — scattering

1. Introduction

The present-day evidence for black holes relies almost entirely on information carried by electromagnetic waves. X-rays play a particular role (Charles, Seward 1995): they are supposed to emerge from gas near a black hole horizon and bring us imprints of physical processes and conditions in the place of their origin and along the ray path. Various spectral and lightcurve patterns have been identified as likely signatures of supermassive black holes in galactic nuclei and stellar-mass black holes. These features presumably arise when matter is accreted from an immediate vicinity of the black hole. The ultimate goal of this effort is to prove the existence of event horizons in 'real' nature, and this way to discover black holes. Clearly, affirmative proof is a great challenge that may still be far in the future. Here we consider a related task, which appears to be somewhat easier on the technical side, though it also still represents an unresolved issue: searching for rays of photons that encircle an ultra-compact star or a black hole.

Accretion disks represent a common way of feeding black holes and generating photons, which then experience strong gravity while travelling to a distant observer (Kato et al. 1998; Krolik 1999). Outside the disk plane, density is much less; however, even regions near the axis are not empty: winds and jets emerge, roughly along the symmetry axis. We address a question whether future observations of polarized time-dependent signal can help us to recognize the effects of light bending, and what features are expected in light curves. To this aim we examine a model of warm clouds moving radially along the symmetry axis. Primary photons from the disk are Thomson-scattered and polarized. We assume that the process takes place near a Schwarzschild black hole, where the higher order (indirect) light rays contribute to the observed radiation flux. The resulting modulation of intensity and polarization magnitude can reach a non-negligible level under a suitable geometrical alignment of the black hole, the cloud, and the observer. We treat the interaction of the cloud with the radiation and gravitational fields in a relativistic framework (Abramowicz et al. 1990; Vokrouhlický, Karas 1991; Keane et al. 2001). This approach provides us with a self-consistent description of the cloud motion and the resulting observed signal. Both ingredients are conveniently expressed in terms of the radiation stress tensor.

There is evidence for jets being formed only a few tens of gravitational radii from a supermassive central black hole (Junor et al. 1999). The emission mechanisms producing the observed high-energy photons (X- and γ-rays) are likely to be non-thermal, but it is not clear whether the synchrotron emission or the inverse Compton emission dominates in each particular source (Harris, Krawczynski 2002). Here, we concentrate on the latter case (within the Thomson approximation), which seems to be relevant for radio-quiet sources with the ambient radiation acting on particles and fluids, and determining their terminal (equilibrium) speed (see Noerdlinger 1974; O'Dell 1981; Sikora, Wilson 1981; Phinney 1982 for original papers). This dynamical influence of the radiation field has been studied further by Sikora et al. (1996), Renaud and Henri (1998), Tajima and Fukue (1998), Fukue and Hachiya (1999), and Watarai and Fukue (1999). Ghisellini et al. (2004) proposed a model of aborted (failed) jets in which colliding clouds and shells occur very near to a black hole and are embedded in strong radiation. According to their scheme, most of the energy dissipation should take place on the symmetry axis of an accretion disk where the individual clouds either move away from the black hole, or fall back. The process of gravitational and radiative acceleration of plasma was also studied by Fukue et al. (2001) and Fukue (2005), who examined the efficiency of collimation toward the disk axis, and applied this model to the case of microquasars.

The effects of strong gravity are significant in this region

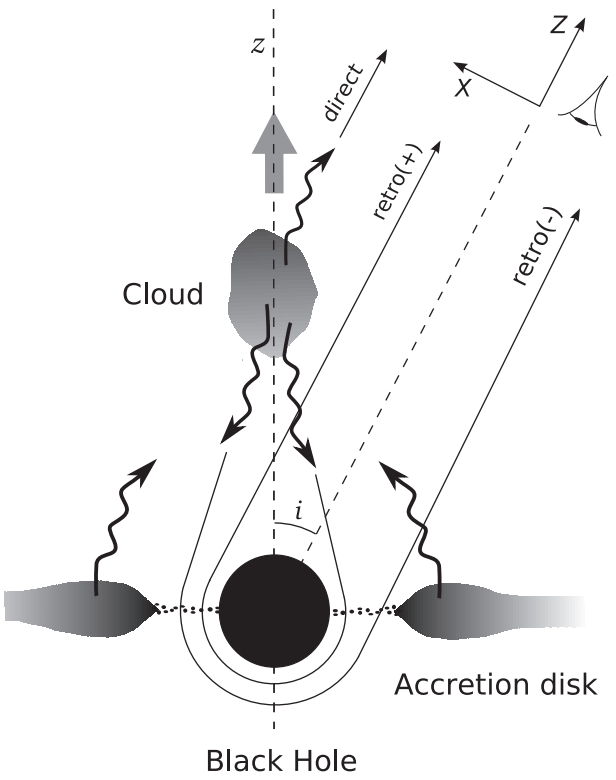

Fig. 1. Geometry of the model. An accretion disk is the source of primary unpolarized light, which is then Thomson scattered on a cloud. The cloud moves radially along the axis, $z \equiv z(t)$, in the radiation field of the disk. The gravity of the central black hole influences the motion of the cloud. The light rays of the primary and scattered photons are also affected. Direct and indirect (retro-lensed) light rays have different degrees of linear polarization, and experience different amplification and the Doppler boosting. The observed lightcurve is produced by all of the rays reaching an observer at view angle i far from the center (along Z-direction). The indirect photons contribute most significantly to the the total signal if the cloud moves toward the black hole and the observer inclination is small.

and the challenge for future techniques is to identify subtle, yet specific patterns in X-ray lightcurves. Polarization studies could help to achieve this goal. Distinct features should arise from multiple trajectories of light rays connecting the source with the observer along several different paths. The rays winding up around the photon circular orbit should experience a characteristic mutual time delay. We discuss the expected features in this paper.

The polarization of light from scattering in winds and jets was examined by various authors. Following the early papers (e.g. Dolan 1967; Angel 1969; Bonometto et al. 1970), Begelman and Sikora (1987) studied the linear polarization of initially unpolarized soft radiation up-scattered by cold electrons in a jet. Beloborodov (1998) examined the case of fast winds outflowing from an accretion-disk slab. He found that the polarization direction depends on the wind velocity; the terminal speed of the outflow plays a critical role. Poutanen (1994) and Celotti and Matt (1994) considered the synchrotron self-Compton mechanism, a likely process that produces polarization wherever magnetic fields interact with relativistic particles. The effect of the electron temperature was also analyzed: it reduces the final magnitude of polarization. Recently, Lazzati et al. (2004) further considered the Compton drag as a conceivable mechanism for polarization in gamma-ray bursts. Horák and Karas (2006) studied the polarization of scattered light from a compact star, taking into account the light-bending effect. In fact, it was demonstrated that retro-lensing images, which clearly require strong gravity, can give rise to specific polarimetric signatures in predicted lightcurves. Here, we develop this model further by considering a non-negligible temperature of the scattering medium and by changing the geometry of the primary source. Since we assume a Keplerian disk as the source, we are able to examine situations that are relevant for accreting black holes.

2. The Model Setup

As a toy-model for non-uniform outflows and aborted jets we consider a cloud of particles that moves through the radiation field of a standard thin accretion disk (Shakura, Sunyaev 1973). The disk defines the equatorial plane $\theta = \pi/2$ of the system. Primary photons from the disk are scattered by electrons in the cloud; they are beamed (preferentially in the direction of the scatterer motion), and polarized by the Thomson mechanism. We adopt the first scattering approximation (small optical depth $\tau \ll 1$ of the cloud is assumed) and restrict the cloud motion to the axis of symmetry, $z \equiv z(t)$. The basic setup of the model is shown in figure 1.

The spacetime metric is (Misner et al. 1973)

$$ds^2 = -\xi\, dt^2 + \xi^{-1} dr^2 + r^2 (d\theta^2 + \sin^2\theta\, d\phi^2), \qquad (1)$$

where $\{\, t, r, \theta, \phi \,\}$ are Schwarzschild coordinates, $\xi(r) \equiv 1 - R_{\rm S}/r$ is the redshift function, $R_{\rm S} \equiv 2GM/c^2$. Geometrized units $c = G = 1$ are used.

The total bolometric luminosity of a standard disk, $L = GM\dot{M}/2R_{\rm in}$, can be scaled by the Eddington luminosity, $L_{\rm E} = 4\pi c G M m_{\rm p}/\sigma_{\rm T}$. We thus define $\Lambda \equiv L/L_{\rm E}$. The corresponding intensity emitted from the disk is

$$I_{\rm d}(r) = \frac{m_{\rm p} c^3}{\sigma_{\rm T} R_{\rm S}} \Lambda I_{\rm d\star}, \quad I_{\rm d\star} \equiv \frac{3\, R_{\rm S}^2 R_{\rm in}}{2\pi r^3} \left(1 - \sqrt{\frac{R_{\rm in}}{r}}\right), \qquad (2)$$

where we denote, by an asterisk, the intensity rescaled to the dimension-less form. Hereafter, the radiation terms will be made dimension-less by scaling them with $(m_{\rm p} c^3/\sigma_{\rm T} R_{\rm S})\,\Lambda$.

Photons travel along null geodesics and give rise to the radiation stress tensor at every point outside the disk plane and above the black-hole horizon. Figure 2 shows the dependence of the components relevant for our calculation on symmetry axis of the black hole — accretion disk system (we employ similar notation for the radiation stress tensor components as e.g. Fukue, Hachiya 1999; Watarai, Fukue 1999).

In spite of the fact that we employ a particular model of a thin accretion disk in this paper, several rather general features are captured in figure 2 that we also expect to shape the radiation field of astrophysically realistic models. These can be summarized as follows:

— The radiation stress tensor vanishes for $z \to \infty$ ($\xi \to 1$) because the angular size of the disk, as observed by distant observers, decreases to zero.

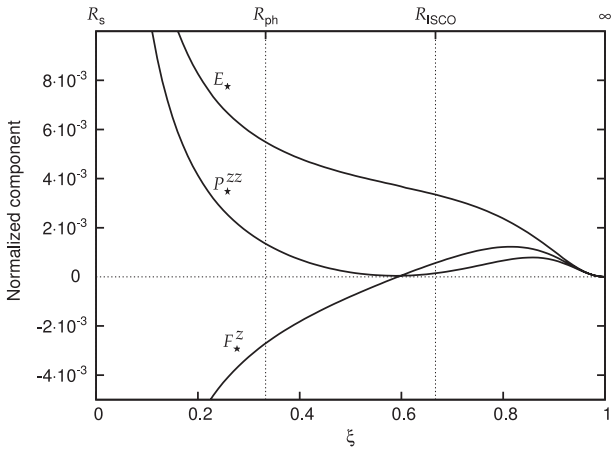

Fig. 2. Normalized components of the radiation stress tensor on the symmetry axis for radiation originating from a standard disk. The inner edge of the disk corresponds to the innermost stable circular orbit, $R_{\rm in} = R_{\rm ISCO} = 3\,R_{\rm S}$; no intervening matter is considered below that radius. The outer edge is at $R_{\rm out} = 10^3\,R_{\rm S}$. The location of the photon circular orbit, $R_{\rm ph} = 1.5\,R_{\rm S}$, is also indicated.

— Far from the centre, the tz-component of the stress tensor (measured by a static observer) is positive; however, this term changes sign at a certain value of the height, z, near above the disk. This effect operates for a static observer inside a photon circular orbit, who intercepts photons falling into the black hole.

— All three components diverge as $z \to R_{\rm S}$ ($\xi \to 0$). Close to the horizon the accretion disk appears again as a point-like source producing an energy density $\propto \xi^{-1}(z)$. Here, two effects act against each other: the gravitational bending of light-rays reduces the solid angle that the disk occupies on the observer local sky by factor $\propto \xi$, whereas the gravitational redshift increases the radiation intensity by a factor $\propto \xi^{-2}$ (blueshift occurs, in fact).

The intensity of scattered light and its polarization are characterized by the Stokes parameters (Chandrasekhar 1960; Rybicky, Lightman 1979). These can be obtained by integrating over all directions, $\boldsymbol{n}_{\rm i}$, of photons incident on scattering particles of the cloud from different points in the disk (Horák, Karas 2006):

$$\overline{I} = \overline{E} + \overline{P}^{ZZ}, \tag{3}$$

$$\overline{Q} = \overline{P}^{YY} - \overline{P}^{XX}, \tag{4}$$

$$\overline{U} = -2\overline{P}^{XY}, \tag{5}$$

where the bars denote quantities in the comoving orthonormal polarization frame, the $\overline{X}$-axis of which is given by projecting the symmetry axis onto the observing plane and the $\overline{Z}$-axis coinciding with the direction of scattered photons. $\overline{P}^{AB}$ are local components of the radiation stress tensor (the spatial part of the energy–momentum tensor $\overline{T}^{(\alpha)(\beta)}$), $\overline{E} \equiv \overline{T}^{(t)(t)}$ is the local energy-density. The values of Stokes parameters (3)–(4) are normalized by $A \equiv 3\tau/16\pi$; $\tau \equiv n_{\rm e}\sigma_{\rm T} R$ is the Thomson optical depth of the cloud in terms of electron density, $n_{\rm e}$; $R \ll R_{\rm S}$ is the radius of the cloud. The polarization is purely linear ($V = 0$) and its magnitude is equal to $\Pi = (\overline{Q}^2 + \overline{U}^2)^{1/2}/\overline{I}$.

3. Polarization from Scattering on Warm Clouds near a Black Hole

So far we have assumed the cloud to be cold, and we did not consider any microscopic (random) motion of the scattering electrons within the cloud volume. Hereafter, in order to account for the electron temperature, we average equations (3)–(5) over the electron distribution, $n(\boldsymbol{\beta}_{\rm e}) = n_{\rm e} f(\gamma_{\rm e})$, in the cloud comoving frame (CCF), where the electron distribution is entirely isotropic and $\gamma_{\rm e} \equiv (1-\beta_{\rm e}^2)^{-1/2}$ is the corresponding Lorentz factor. The Stokes parameters are first evaluated in the local electron comoving frame (ECF), Lorentz transformed to the CCF, and the result is averaged over random velocities of the electrons. We obtain

$$\overline{I} = (1+\mathcal{A})\left(\overline{E} + \overline{P}^{ZZ}\right) + \mathcal{B}\left(\overline{E} - 3\overline{P}^{ZZ}\right) - 2\mathcal{A}\overline{F}^{Z}, \tag{6}$$

$$\overline{Q} = \overline{P}^{YY} - \overline{P}^{XX}, \tag{7}$$

$$\overline{U} = -2\overline{P}^{XY}, \tag{8}$$

where F^Z is the radiation flux component measured in the direction of the photon after scattering. We introduce the mean values

$$\mathcal{A} \equiv \frac{4}{3}\left\langle \gamma_{\rm e}^2 \beta_{\rm e}^2 \right\rangle, \qquad \mathcal{B} \equiv 1 - \left\langle \frac{\ln[\gamma_{\rm e}(1+\beta_{\rm e})]}{\beta_{\rm e}\gamma_{\rm e}^2} \right\rangle; \tag{9}$$

$\langle x \rangle \equiv \int x f(\gamma_{\rm e}) d\gamma_{\rm e}$ denotes averaging over the electron energy distribution; see Horák (2005) for details of the derivation of equations (6)–(8).

The Lorentz boost from CCF to the static frame introduces the familiar factor $\mathcal{D}^4$, where $\mathcal{D} = \gamma^{-1}(1 - \beta\cos\vartheta)^{-1}$ is the Doppler factor, $\gamma = (1-\beta^2)^{-1/2}$, β is the cloud bulk velocity and ϑ is the angle between this velocity and the scattered photon direction:

$$I = \mathcal{D}^4 \overline{I}, \qquad Q = \mathcal{D}^4 \overline{Q}, \qquad U = \mathcal{D}^4 \overline{U}. \tag{10}$$

In this way the frequency-integrated Stokes parameters are found in terms of the radiation stress-tensor components. The relation between the CCF components ($\overline{E}, \overline{F}^A, \overline{P}^{AB}$) and the static frame components (E, F^a, P^{ab}) is

$$\overline{P}^{XX} = \mathcal{D}^2\left[P^{xx}(\cos\vartheta - \beta)^2 + \gamma^2\Delta\sin^2\vartheta\right], \tag{11}$$

$$\overline{P}^{ZZ} = \mathcal{D}^2\left[P^{xx}\sin^2\vartheta + \gamma^2\Delta(\cos\vartheta - \beta)^2\right], \tag{12}$$

$$\overline{P}^{YY} = \overline{P}^{yy}, \tag{13}$$

$$\overline{E} = \gamma^2\left(E - 2\beta F^z + \beta^2 P^{zz}\right), \tag{14}$$

$$\overline{F}^Z = \mathcal{D}\gamma^2(\cos\theta - \beta)\,W, \tag{15}$$

where we denote $\Delta = \beta^2 E - 2\beta F^z + P^{zz}$ and $W = (1+\beta^2)F^z - \beta(E + P^{zz})$. Axial symmetry ensures that $\overline{P}^{XY}$ vanishes for the primary radiation field originating from the disk and impinging on the cloud.

The properties of the scattered signal in the static frame of course depend on the motion of the scatterer, which itself

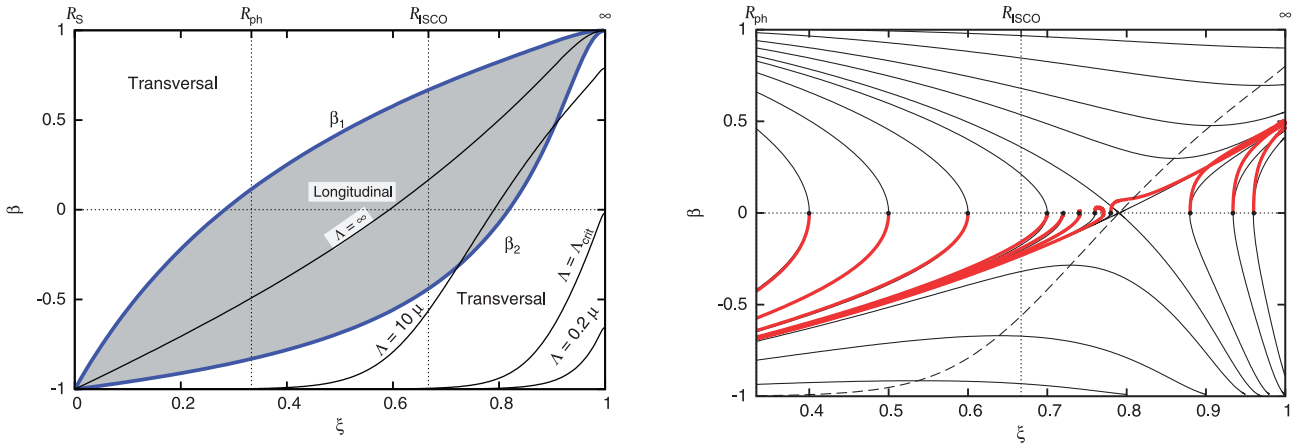

Fig. 3. Left: critical velocities of the cloud motion, $\beta_1(\xi)$ and $\beta_2(\xi)$, at which the observed polarization vector changes its orientation between the longitudinal (inside the shaded region) and the transversal one. The saturation curves, $\beta \equiv \beta_0(\xi)$, are also plotted and labelled by the values of the normalized luminosity, Λ (for $\Lambda = \Lambda_{\rm crit}$ the saturation velocity vanishes at infinity). Right: several examples of possible trajectories of a warm electron cloud (thick curves). The initial condition is $\beta(t_0) = 0$; the values of $\xi(t_0)$ are indicated by a circle. A monoenergetic distribution of scattering electrons was assumed, $f(\gamma_{\rm e}) = \delta(\gamma_{\rm e} - \langle\gamma_{\rm e}\rangle)$. Cold cloud trajectories are shown for the sake of a comparison (thin solid curves). The saturation curve is also plotted (dashed), corresponding to the luminosity parameter, $\Lambda = 10\,\mu$.

results from an interplay of the acceleration mechanisms acting on the cloud. In our model the total four-force, f^α, is a superposition of the radiation and inertial terms. The radiation term is

$$f^\alpha = -\sigma_{\rm T} n_{\rm e}\, \delta\mathcal{V} \left[\mathcal{C} T^{\alpha\beta} u_\beta - (\mathcal{A} + \mathcal{C}) T^{\rho\sigma} u_\rho u_\sigma u^\alpha\right], \qquad (16)$$

where $\delta\mathcal{V}$ is the cloud volume, $\mathcal{C} \equiv 1 + (1/2)\mathcal{A}$. The change of the cloud internal energy by cooling is

$$\frac{d\langle\gamma_{\rm e}\rangle}{ds} = -\gamma\, \mathcal{A}\Lambda\mu \left(E_\star - 2\beta F^z_\star + \beta^2 P^{zz}_\star\right), \qquad (17)$$

where we express the proper time, s, in units of $R_{\rm S}/c$, and we denote $\mu \equiv m_{\rm p}/m_{\rm e} \simeq 1$ (for electron–proton plasma) or $\mu \simeq 10^3$ (for electron–positron plasma). The parameterisation by μ allows us to consider different types of plasma. However, we note that the radiation field of a standard disk alone is unable to efficiently accelerate protons, and so the case of an electron–positron plasma seems to be a more relevant application here (Fukue 2005).

The dynamics of the cloud as a whole is governed by the equation of motion in the form

$$\frac{d\beta}{ds} = \langle\gamma_{\rm e}\rangle^{-1} \mathcal{C}\Lambda\mu \left[(1+\beta^2)F^z_\star - \beta(E_\star + P^{zz}_\star)\right] - \frac{R_{\rm S}}{2\gamma z^2 \xi^{1/2}}, \qquad (18)$$

which also includes the black hole gravity. The last two equations couple the cloud trajectory with the evolution of its internal temperature. In order to close the set of equations we need to assume a specific form of the electron energy distribution $f(\gamma_{\rm e})$.

In the case of cold clouds ($\mathcal{A} = 0$, $\mathcal{C} = 1$) the dynamics is characterized by the saturation velocity, $\beta_0(\xi)$, to which particles are asymptotically accelerated if inertial effects are small compared to the radiation force (Sikora, Wilson 1981; Icke 1989). This condition corresponds to the limit of $\Lambda \to \infty$, $d\beta/ds = 0$. We thus obtain

$$\beta(z) \to \beta_0 = \sigma - \sqrt{\sigma^2 - 1}, \qquad \sigma \equiv \frac{E_\star + F^z_\star}{2F^z_\star}. \qquad (19)$$

Further, for polarization there are two critical velocities, $\beta_1(\xi)$ and $\beta_2(\xi)$, at which the polarization vector changes its orientation between the transversal and longitudinal one (this can be seen from the condition $\overline{Q} = 0$). Similar effect of polarization direction changing with the velocity of the scattering medium was studied by Beloborodov (1998; for scattering in fast outflows from accretion disks) and Horák and Karas (2006; for radially moving clouds near a compact star). This behavior is demonstrated in the left panel of figure 3. The right panel shows the corresponding influence of the radiation cooling of the cloud on its bulk motion.

From equation (18) we find that the motion of warm clouds is governed by the same equation as cold ones, provided that the normalized luminosity is rescaled,

$$\Lambda \to \Lambda' \equiv \langle\gamma_{\rm e}\rangle^{-1}\mathcal{C}\Lambda. \qquad (20)$$

In other words, by keeping the disk luminosity at a constant value of the Eddington parameter, the cooling (17) gives rise to trajectories gradually deviating from the corresponding cold-cloud limit.

The effect of changing temperature is such that the saturation velocity curve gradually moves across the (β, ξ)-plane. This helps us to understand the form of trajectories, which create loops (see figure 3, right panel). The critical point is given by the condition $\beta = 0$, $0 < \xi < \infty$ and it defines the distance where equilibrium between the radiation and the gravity can be reached. This is a saddle-type point, characteristic of an unstable equilibrium, which makes the system behavior qualitatively different from the case with a central star as a source of primary irradiation (cp. with the critical points examined in Abramowicz et al. 1990). Our result here resembles the case of clouds with non-constant mass, discussed by Keane et al. (2001).

We can now find the Stokes parameters of scattered light

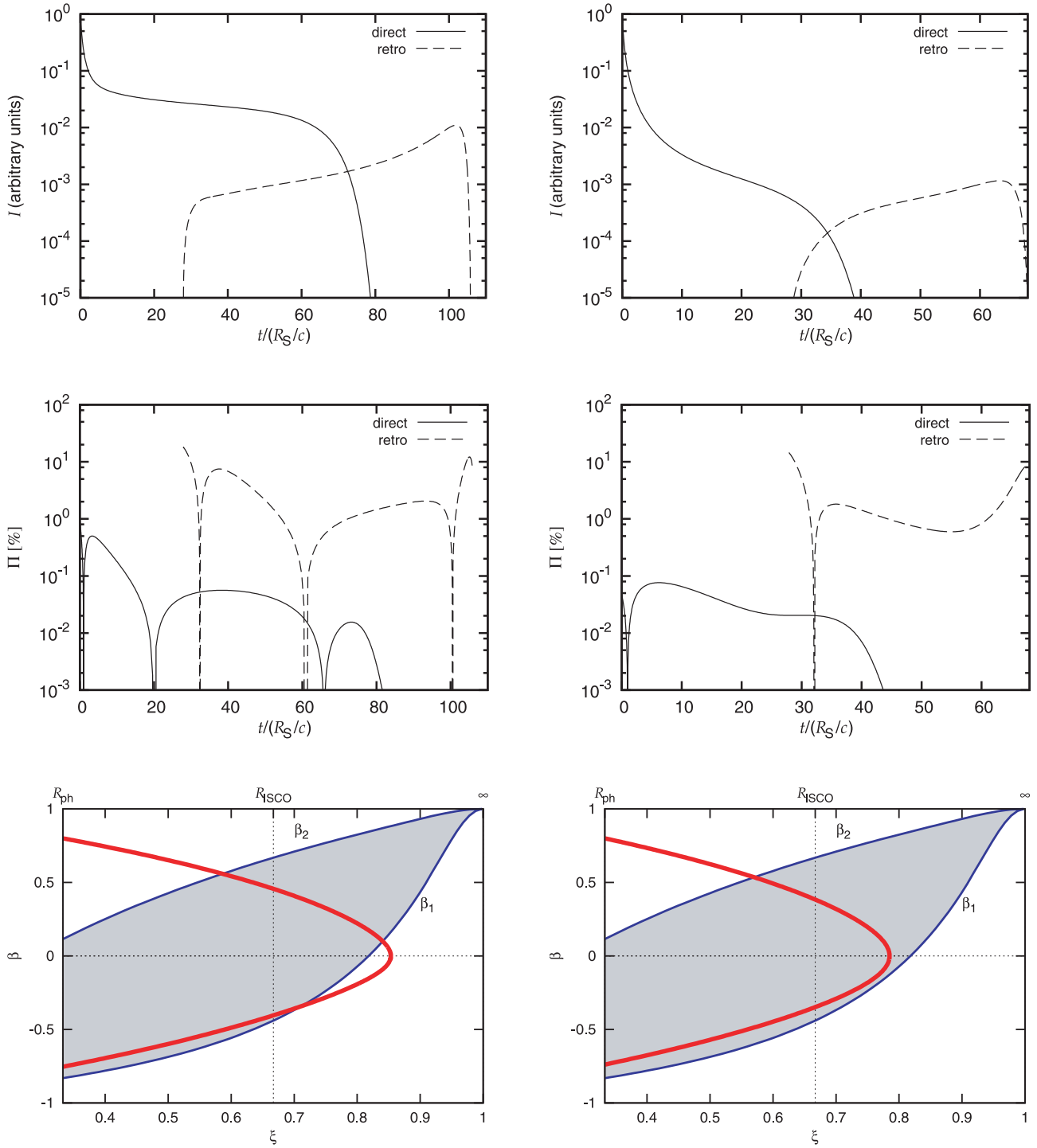

Fig. 4. Comparison between two typical cases with the identical initial conditions, except for the cloud temperature: a cold cloud (left panels, $\langle\gamma_e\rangle = 1$) versus a warm cloud (right panels, $\langle\gamma_e\rangle = 3$ at start). Examples are shown of the time behavior of the observed intensity (top row) and the magnitude of polarization (middle row). Contributions of the retro-lensing images have been summed together and plotted (by a dashed line); they are clearly distinguished from the signal produced by the direct-image photons (solid line). The retro-lensing photons arrive with a certain time delay with respect to the direct photons. The delay is caused by photons taking different paths and circling at $r \simeq R_{\rm ph}$ (the effect can be recognized by comparing the relative time shift of the features). We also show, in the bottom row, the corresponding velocity profile, $\beta(\xi)$, of the cloud motion. The temperature evolution is given by solving equation (17) along the trajectory: the warm cloud cools down to $\langle\gamma_e\rangle = 1.3$ along its entire track. Polarization vanishes at the moment when the cloud crosses one of the curves $\beta_1(\xi)$, $\beta_2(\xi)$. In both cases the view angle was $i = 5^\circ$ and the disk luminosity was $\Lambda = 2$. The initial distance was $z(t_0) = R_{\rm ph}$ (i.e. $\xi = 1/3$), and $\beta(t_0) = 0.8$.

along the cloud path. When determining the temporal evolution of the observed intensity and polarization we first consider three images in the observed radiation: a direct (zeroth-order) image and two first-order images. The latter are retro-lensing images formed by rays making a single round about the black hole by an angle of $\Phi = 2\pi \pm i$, where i is the observer inclination (we denote the retro-lensing images by $\pm$ signs to indicate that they wind up in the opposite directions around the black hole). Since the higher order images give a progressively weaker contribution to the final signal, we can safely neglect them. The retro-lensing photons give rise to peaks in the observed signal occurring with a characteristic mutual time lag after the direct-image photons. The duration of these features is very short — comparable to the light crossing time — and the time span of the plots can therefore be scaled by $t_{\rm lc} \simeq 1.5 \times 10^{-4} M/(10\,M_\odot)$ [s].

Typical profiles of the resulting lightcurves and polarization curves are shown in figure 4. Here, we notice the difference in the lightcurve profiles and the the polarization curves, which is caused by an effect of the cloud initial temperature and its gradual cooling. The contribution of the retro-lensing images to the total observed flux is maximum when the scatterer, the black hole and the observer are well-aligned ($i \to 0$) and the scatterer moves towards black hole ($\beta \to -1$). In this situation a non-negligible fraction of photons are scattered toward being on the light circular photon orbit; their energy is Doppler boosted, and eventually they are redirected toward the observer. On the other hand, the polarization magnitude attains its maximum value in a slightly different direction, whereas, for symmetry reasons, Π vanishes for a strictly aligned observer. The direct image photons are of course most intense in the opposite case ($\beta \to 1$), and so there is an interplay of different orders of the images sensitive to the model parameters.

Identifying the short-duration features in lightcurves could help to confirm the existence of the photon circular orbit around the central body, for which black holes are the most likely cause. Polarimetric resolution provides additional information about the source, and it could be used to constrain the parameters of the black hole.

4. Discussion and Conclusions

In X-rays, future polarimeters could be employed to probe jets and winds in strong gravitational fields of the central compact object. Polarimetry is a powerful tool that can provide additional information, which would be difficult to obtain by other techniques, such as traditional photometry and spectroscopy. In this way polarimetry helps to discriminate between different geometries and physical states of sources where accretion processes are accompanied by fast radial motion of the blobs of material. Naturally, this goal would require sufficient sensitivity in X-rays; the scattered signal is mixed with primary photons, which reduces the final polarization. We have seen that the predicted features are flashing for only a brief period of time, and the maximum polarization degree is typically a few percent or less.

In order to allow an analytical treatment we employed various simplifications: we considered the bolometric quantities and the Thomson cross-section for the scattering of primary photons on electrons (rather than Compton scattering and the Klein–Nishina cross-section; see Melia, Königl 1989; Skibo et al. 1994; Madau, Thompson 2000). We also assumed that the flow is not magnetically dominated, although astrophysically realistic models require magnetohydrodynamic effects to be taken into account (Begelman et al. 1984; Beskin et al. 2004). The effects of general relativity were taken into account in the limit of the non-rotating black hole spacetime (we neglected the effects of frame-dragging for the sake of simplicity; cf. Vokrouhlický, Karas 1991). Likewise, we adopted the simplest possible parameterization of the disk emissivity via the standard Shakura–Sunyaev model; this could be improved by including relativistic effects (Page, Thorne 1974) and a more realistic description of the disk itself. These changes will be necessary to provide quantitative and astrophysically realistic results for the polarization degree; however, we do not expect any qualitative change regarding the signature of indirect photons. The predicted polarization is either parallel or perpendicular to the projection of cloud velocity onto the observing plane.

We gratefully acknowledge fruitful discussions at the Institute of Theoretical Physics in Prague, and we give thanks for helpful comments that we have received from the referee. We also acknowledge the financial support from the Academy of Sciences (ref. IAA 300030510) and from the Czech Science Foundation (refs. 205/03/H144 and 205/06/P415). The Astronomical Institute has been operated under the project AV0Z10030501.

References

Abramowicz, M. A., Ellis, G. F. R., & Lanza, A. 1990, ApJ, 361, 470
Angel, J. R. P. 1969, MNRAS, 158, 219
Begelman, M. C., Blandford, R. D., & Rees, M. J. 1984, Rev. Mod. Phys., 56, 255
Begelman, M. C., & Sikora, M. 1987, ApJ, 322, 650
Beloborodov, A. M. 1998, ApJ, 496, L105
Beskin, V. S., Zakamska, N. L., & Sol, H. 2004, MNRAS, 347, 587
Bonometto, S., Cazzola, P., & Saggion, A. 1970, A&A, 7, 292
Celotti, A., & Matt, G. 1994, MNRAS, 268, 451
Chandrasekhar, S. 1960, Radiative Transfer (New York: Dover)
Charles, P. A., & Seward, F. D. 1995, Exploring the X-Ray Universe (Cambridge: Cambridge University Press)
Dolan, J. F. 1967, Space Sci. Rev., 6, 579
Fukue, J. 2005, PASJ, 57, 691
Fukue, J., & Hachiya, M. 1999, PASJ, 51, 185
Fukue, J., Tojyo, M., & Hirai, Y. 2001, PASJ, 53, 555
Ghisellini, G., Haardt, F., & Matt, G. 2004, A&A, 413, 535
Harris, D. E., & Krawczynski, H. 2002, ApJ, 565, 244
Horák, J. 2005, in Proc. Workshop on Processes in the Vicinity of Black Holes and Neutron Stars, Vol. 6/7, ed. S. Hledík & Z. Stuchlík (Opava: Silesian University), 63
Horák, J., & Karas, V. 2006, MNRAS, 365, 813
Icke, V. 1989, A&A, 216, 294
Junor, W., Biretta, J. A., & Livio, M. 1999, Nature, 401, 891

Kato, S., Fukue, J., & Mineshige, S. 1998, Black-Hole Accretion Disks (Kyoto: Kyoto University Press)
Keane, A. J., Barrett, R. K., & Simmons, J. F. L. 2001, MNRAS, 321, 661
Krolik, J. H. 1999, Active Galactic Nuclei: From the Central Black Hole to the Galactic Environment (Princeton: Princeton University Press)
Lazzati, D., Rossi, E., Ghisellini, G., & Rees, M. J. 2004, MNRAS, 347, L1
Madau, P., & Thompson, C. 2000, ApJ, 534, 239
Melia, F., & Königl, A. 1989, ApJ, 340, 162
Misner, C. W., Thorne, K. S., & Wheeler, J. A. 1973, Gravitation (San Francisco: Freeman)
Noerdlinger, P. D. 1974, ApJ, 192, 529
O'Dell, S. L. 1981, ApJ, 243, L147
Page, D. N., & Thorne, K. S. 1974, ApJ, 191, 499
Phinney, E. S. 1982, MNRAS, 198, 1109
Poutanen, J. 1994, ApJS, 92, 607
Renaud, N., & Henri, G. 1998, MNRAS, 300, 1047
Rybicki, G. B., & Lightman, A. P. 1979, Radiative Processes in Astrophysics (New York: Wiley)
Shakura, N. I., & Sunyaev, R. A. 1973, A&A 24, 337
Sikora, M., Sol, H., Begelman, M. C., & Madejski, G. M. 1996, MNRAS, 280, 781
Sikora, M., & Wilson, D. B. 1981, MNRAS, 197, 529
Skibo, J. G., Dermer, C. D., & Kinzer, R. L. 1994, ApJ, 426, L23
Tajima, Y., & Fukue, J. 1998, PASJ, 50, 483
Vokrouhlický, D., & Karas, V. 1991, A&A, 252, 835
Watarai, K., & Fukue, J. 1999, PASJ, 51, 725